

Supporting Information

Investigation of Vanadium(III) and Vanadium(IV) Compounds Supported by the Linear Diaminebis(aryloxido) Ligands. Correlation Between Structures and Magnetic Properties.

Zofia Janas,^{*a} Julia Jezierska,^a Andrew Ozarowski,^{*b} Alina Bieńko,^{*a} Tadeusz Lis,^a Adam Jezierski^a and Marta Krawczyk^c

^a Faculty of Chemistry, University of Wrocław, 14, F. Joliot-Curie, 50-383 Wrocław, Poland, e-mail: zofia.janas@chem.uni.wroc.pl

^b National High Magnetic Field Laboratory, Florida State University, 1800 E. Paul Dirac Drive, Tallahassee, FL 32310 USA, e-mail: ozarowski@magnet.fsu.edu

^c Faculty of Pharmacy, Wrocław Medical University, 211 Borowska, 50-556 Wrocław, Poland

Contents

- Figure S1.** Arrangement of molecules of **1** forming a chain stretching along [001] direction.
- Figure S2.** Packing diagram for **2**.
- Figure S3.** Fragment of packing diagram for **2** showing C–H··· π intermolecular interactions.
- Figure S4.** The molecular structure of **3**.
- Figure S5.** Arrangement of molecules of **3** viewed down [010] direction.
- Figure S6.** Packing diagram presenting selected molecules of **4** arranged in layers parallel to the (010) plane.
- Figure S7.** The molecular structure of **5**·2CH₃CN.
- Figure S8.** Arrangement of molecules of **5** viewed down [001] direction.
- Figure S9.** A chain of molecules of **5** held together by C–H··· π interactions and hydrogen bonds.
- Figure S10.** Packing diagram for **6** viewed down [010] direction.
- Figure S11.** C–H··· π interactions in **6**.
- Figure S12.** EPR frozen solution spectra (at 77 K) of compounds **3–7**
- Figure S13.** The χ_{MT} vs T product after subtracting TIP from the experimental data.
- Figure S14.** Dihedral angle between the two V₂O₂ planes for complexes **3–5**.
- Figure S15.** The HFEP spectrum of **1**.

Figure S16. DC magnetic data for **1**, **2** and **6**, **7**. Left – () □MT and (○) □M. Right – field dependence of the magnetization per formula unit. The solid lines are calculated using the PHI program.

Table S1. Crystal and structure refinement data for **1**, **2**·0.25CH₃CN, **3**, **4**·2CH₃CN, **5**·2CH₃CN and **6**.

Table S2. Selected Bond Lengths (Å) and Angles (°) for **1** and **2**·0.25CH₃CN.

Table S3. Selected Bond Lengths (Å) and Angles (°) for **3**, **4**·2CH₃CN, **5**·2CH₃CN and **6**.

Table S4. Geometry of the intermolecular hydrogen bonds in **2**.

Table S5. Geometry of C–H···π interactions in **2**.

Table S6. Geometry of the intermolecular hydrogen bonds in **1**.

Table S7. Geometry of C–H···π interactions in **1**.

Table S8. Geometry of C–H···π interactions in **3**.

Table S9. Geometry of intermolecular hydrogen bonds in **4**.

Table S10. Geometry of C–H···π interactions in **4**.

Table S11. Geometry of C–H···π interactions in **5**.

Table S12. Geometry of intermolecular hydrogen bonds in **5**.

Table S13. Geometry of π···π interactions in **6**.

Table S14. Geometry of C–H···π interactions in **6**.

Table S1. Crystal and structure refinement data for **1**, **2**·0.25CH₃CN, **3**, **4**·2CH₃CN, **5**·2CH₃CN and **6**.

symbol of the structure	1	2 ·0.25CH ₃ CN	3	4 ·2CH ₃ CN	5 ·2CH ₃ CN	6
empirical formula	C ₂₅ H ₃₃ N ₂ O ₄ V	C ₂₇ H ₃₇ N ₂ O ₄ V·0.25C ₂ H ₃ N	C ₆₈ H ₁₀₈ N ₄ O ₆ V ₂	C ₄₄ H ₅₈ N ₆ O ₆ V ₂	C ₄₀ H ₄₆ Cl ₄ N ₆ O ₆ V ₂	C ₂₂ H ₃₀ N ₂ O ₃ V
formula weight	476.47	514.79	1179.46	868.84	950.51	421.42
crystal size [mm ³]	0.49 x 0.23 x 0.06	0.60 x 0.13 x 0.06		0.28x0.13x0.08	0.18x0.27x0.43	0.60x0.53x0.40
crystal system	monoclinic	monoclinic	monoclinic	monoclinic	monoclinic	monoclinic
space group	<i>P2₁/c</i>	<i>P2₁/n</i>	<i>P2₁/n</i>	<i>P2₁/n</i>	<i>P2₁/n</i>	<i>P2₁/n</i>
a [Å]	12.011(3)	13.237(3)	20.300(9)	13.687(4)	13.557(4)	13.376(5)
b [Å]	14.728(3)	15.650(4)	8.107(2)	11.336(5)	11.269(3)	11.010(3)
c [Å]	13.307(3)	25.711(7)	22.043(10)	13.947(4)	13.829(5)	15.427(6)
β [°]	97.28(2)	99.83(3)	112.25(5)	94.91(3)	94.93(3)	113.00(4)
V [Å ³]	2335.0(9)	5248(2)	3358(3)	2156.0(13)	2104.9(11)	2091.3(14)
Z	4	8	2	2	2	4
density (calcd) [g·m ⁻³]	1.355	1.303	1.167	1.338	1.500	1.338
F(000)	1008	2188	1276	916	980	892
coeff. μ [mm ⁻¹]	0.459	0.414	0.329	0.487	0.752	0.499
T [K]	100(2)	103(2)	150(2)	125(2)	90(2)	101(2)
λ [Å]	0.71073	0.71073	0.71073	0.71073	0.71073	0.71073
reflections coll., independ.	6668, 15428	12638, 42392	7341, 26589	6054, 12067	5777, 10198	10167, 34826
R _{int}	0.028	0.083	0.12	0.097	0.12	0.056
data/restraints/parameters	6668/0/295	12638/0/651	7341/0/389	6054/0/267	5777/0/265	10167/0/259
final R indices	0.039	0.051	0.074	0.057	0.046	0.048
(I > 2σ(I))	0.087	0.113	0.166	0.098	0.095	0.138
final R ₁ , wR (all data)	0.055, 0.094	0.089, 0.120	0.125, 0.200	0.097, 0.112	0.071, 0.108	0.055, 0.143
GOF on F ²	1.021	1.004	1.038	1.032	1.026	1.093
CCDC numbers	1997038	1997039	1997040	1997041	1997042	1997043

Table S2. Selected Bond Lengths (Å) and Angles (°) for **2** and **2**·0.25CH₃CN.

	1	2^a	2^b
V–O1	1.9317(12)	1.9314(18)	1.9425(17)
V–O2	1.9263(12)	1.9315(17)	1.9282(17)
V–O3	2.0072(11)	1.9717(17)	1.9945(17)
V–O4	1.9817(11)	2.0176(18)	1.9837(19)
V–N1	2.2253(13)	2.231(2)	2.189(2)
V–N2	2.1850(13)	2.173(2)	2.205(2)
O2–V–O1	171.85(5)	171.09(7)	171.94(8)
O2–V–O4	96.47(5)	87.49(7)	91.92(7)
O1–V–O4	91.67(5)	91.20(8)	96.14(7)
O2–V–O3	89.75(4)	97.67(7)	89.58(7)
O1–V–O3	90.65(5)	91.14(7)	90.64(7)
O4–V–O3	89.95(5)	89.85(7)	90.76(7)
O2–V–N2	88.39(5)	87.59(8)	86.25(7)
O1–V–N2	91.14(5)	94.06(8)	85.72(7)
O4–V–N2	90.57(5)	174.41(8)	172.13(7)
O3–V–N2	178.12(5)	88.19(7)	96.88(8)
O2–V–N1	85.82(5)	86.53(7)	93.13(8)
O1–V–N1	86.05(5)	85.06(7)	86.48(7)
O4–V–N1	172.20(5)	100.84(7)	90.53(7)
O3–V–N1	97.52(5)	168.71(8)	176.96(7)
N2–V–N1	82.03(5)	81.49(8)	81.94(8)

Table S3. Selected Bond Lengths (Å) and Angles (°) for **3**, **4**·2CH₃CN, **5**·2CH₃CN and **6**.

	3	4	5	6
V1–O1	1.921(2)	1.9148(16)	1.9268(16)	1.8983(12)
V1–O2	1.607(2)	1.6115(19)	1.6108(15)	1.6025(9)
V1–O3	2.017(2)	2.0174(16)	2.0236(16)	1.9219(10)
V1–O3	2.046(2)	2.0377(16)	2.0476(16)	–
V1–N1	2.225(3)	2.2166(19)	2.210(2)	2.2003(9)
V1–N2	2.440(3)	2.417(2)	2.3979(18)	2.1672(9)
V...V ⁱ	3.2433(18)	3.2488(12)	3.2540(13)	–
O2–V1–O1	104.06(11)	103.77(8)	103.06(7)	113.00(5)
O2–V1–O3	104.10(11)	103.96(7)	103.68(7)	109.04(5)
O1–V1–O3	88.13(10)	87.83(7)	88.21(7)	83.57(5)
O1–V1–O3	154.85(9)	154.84(7)	155.90(6)	–
O3–V1–O3	74.11(10)	73.52(7)	73.88(7)	–
O2–V1–N1	87.36(12)	88.34(8)	88.34(7)	99.63(5)
O1–V1–N1	89.44(11)	90.01(7)	90.06(7)	88.49(4)
O3–V1–N1	168.53(9)	167.68(7)	167.94(6)	151.13(3)
O3–V1–N1	104.41(10)	104.58(7)	104.05(7)	–
O2–V1–N2	160.97(12)	162.25(7)	163.02(7)	105.99(5)
O1–V1–N2	84.31(10)	84.55(7)	84.77(6)	140.81(3)
O3–V1–N2	93.10(10)	91.86(7)	91.48(6)	87.54(4)
O3–V1–N2	79.14(10)	79.46(6)	79.81(6)	–
N1–V1–N2	75.51(10)	75.86(7)	76.48(6)	81.23(4)
V1–O3–V1	105.89(10)	106.48(7)	106.12(7)	–

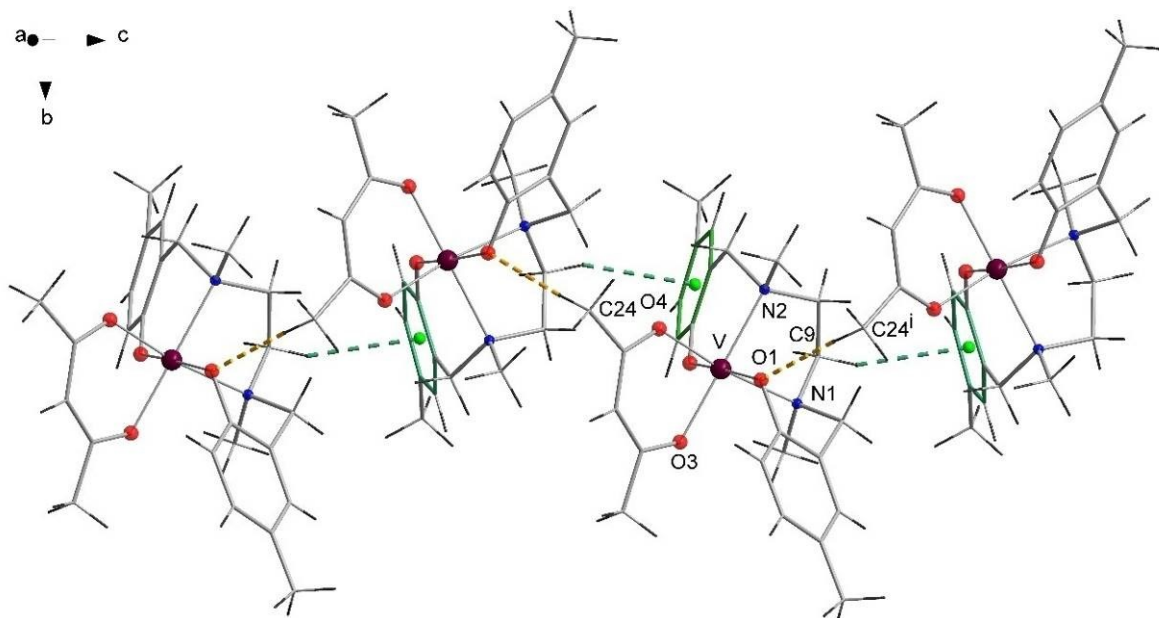


Figure S1. Arrangement of molecules **1** forming a chain stretching along [001] direction. C24–H24C \cdots O1ⁱ hydrogen bonds are marked by yellow dashed lines. For C–H \cdots π interactions of C9–H9B \cdots Cg6ⁱ the centroid of the aromatic ring are shown as a light green dummy atom and the ring along with the H \cdots π distance are marked by green line. Symmetry codes: [i] x, 1/2–y, 1/2+z.

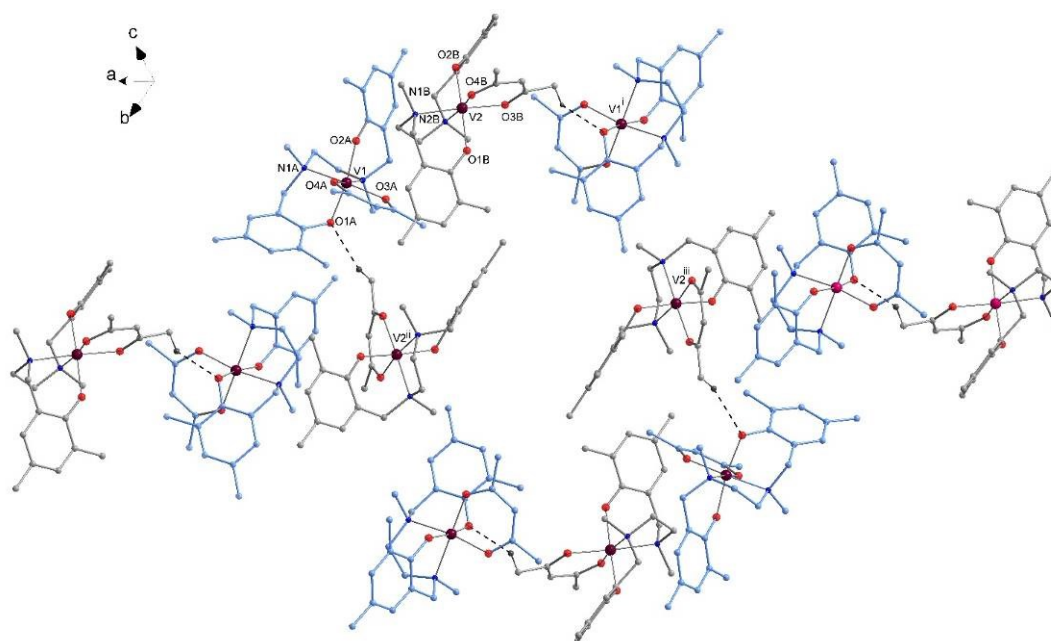


Figure S2. Packing diagram for **2**. H atoms engaged in the intermolecular hydrogen bond interactions are marked. The remaining hydrogen atoms and molecules of acetonitrile have been

removed from the drawing for clarity. Symmetry codes: [i] $1/2-x, 1/2+y, 1/2-z$; [ii] $1/2-x, -1/2+y, 1/2-z$; [iii] $-1/2+x, 1/2-y, -1/2+z$.

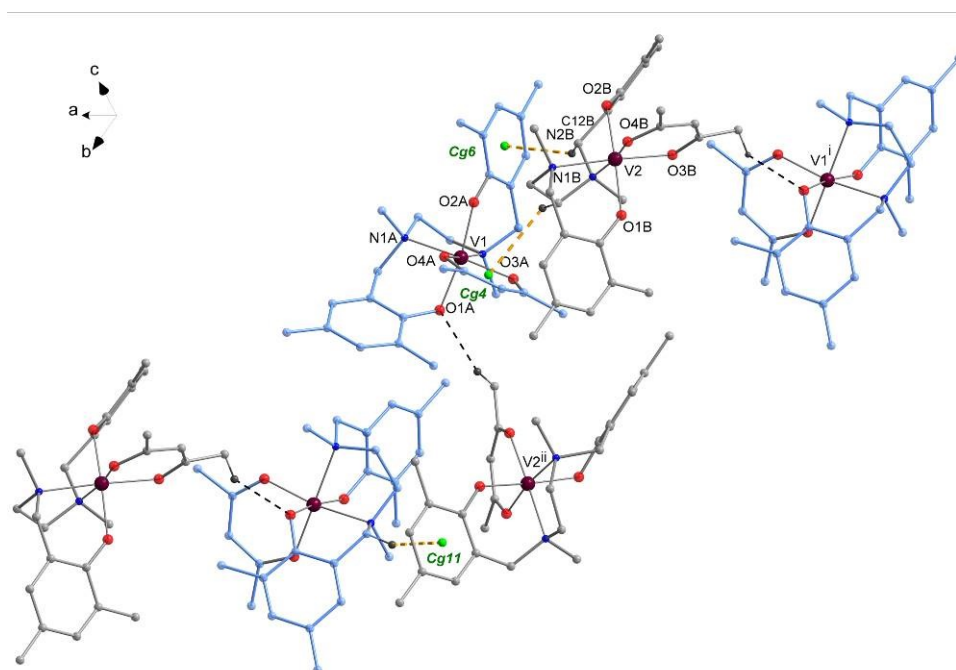


Figure S3. Fragment of packing diagram for **2** showing the C–H \cdots π intermolecular interactions (marked by yellow dashed line; centroids of aromatic rings are shown as light-green dummy atoms). H atoms engaged in the intermolecular hydrogen bond interactions are marked. The remaining hydrogen atoms and molecules of acetonitrile have been removed from the drawing for clarity. Symmetry codes: [i] $1/2-x, 1/2+y, 1/2-z$; [ii] $1/2-x, -1/2+y, 1/2-z$; [iii] $-1/2+x, 1/2-y, -1/2+z$.

Table S4. Geometry of the intermolecular hydrogen bonds in **2**.

D–H \cdots A	D–H (Å)	H \cdots A (Å)	D \cdots A (Å)	\angle (D–H \cdots A) (°)
C23B–H23D \cdots O1A ⁱⁱ	0.98	2.48	3.350(3)	147

Symmetry codes: [ii] $1/2-x, -1/2+y, 1/2-z$

Table S5. Geometry of C–H \cdots π interactions in **2**.

C–H \cdots π	H \cdots Cg (Å)	C \cdots Cg (Å)	\angle (C–H \cdots Cg) (°)
C7A–H7A2 \cdots Cg11 ⁱ	2.75	3.58	142
C2–H2A \cdots Cg12	2.60	3.35	133
C2–H2C \cdots Cg12 ⁱⁱ	2.88	3.54	125
C10B–H10D \cdots Cg4	2.96	3.52	116
C12B–H12D \cdots Cg6	2.88	3.64	135

C22A–H22B···Cg4 2.71 3.56 145

Symmetry codes: [i] 1+x, y, z; [ii] 1-x, -y, 1-z

Cg4 [V1/O3A/C24A/C25A/C26A/O4A]; Cg6 [C13/C14/C15/C16/C17/C18];
Cg11 [C1B/C2B/C3B/C4B/C5B/C6B]; Cg12 [C13B/C14B/C15B/C16B/C17B/C18B].

C2 – a C atom of the methyl group from acetonitrile

Table S6. Geometry of the intermolecular hydrogen bonds in **1**.

D–H···A	D–H (Å)	H···A (Å)	D···A (Å)	<(D–H···A) (°)
C24–H24C···O1 ⁱ	0.98	2.51	3.487(2)	176

Symmetry codes: [i] x, 1/2-y, 1/2+z

Table S7. Geometry of C–H··· π interactions in **1**.

C–H··· π	H···Cg (Å)	C···Cg (Å)	<(C–H···Cg) (°)
C9–H9B···Cg6 ⁱ	2.73	3.66	157

Symmetry codes: [i] x, 1/2-y, 1/2+z

Cg6 [C13/C14/C15/C16/C17/C18]

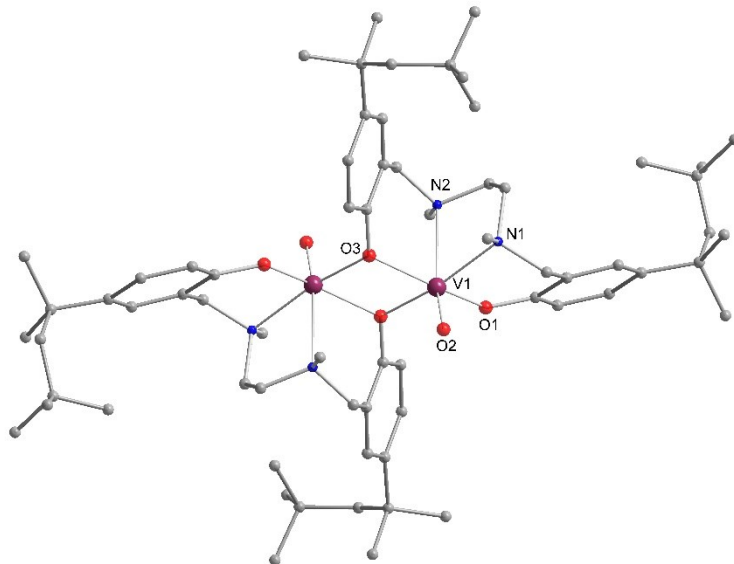


Figure S4. The molecular structure of **3** with crystallographic numbering of the donor atoms. Only the higher occupation component of the disordered part was depicted. H atoms have been omitted for clarity.

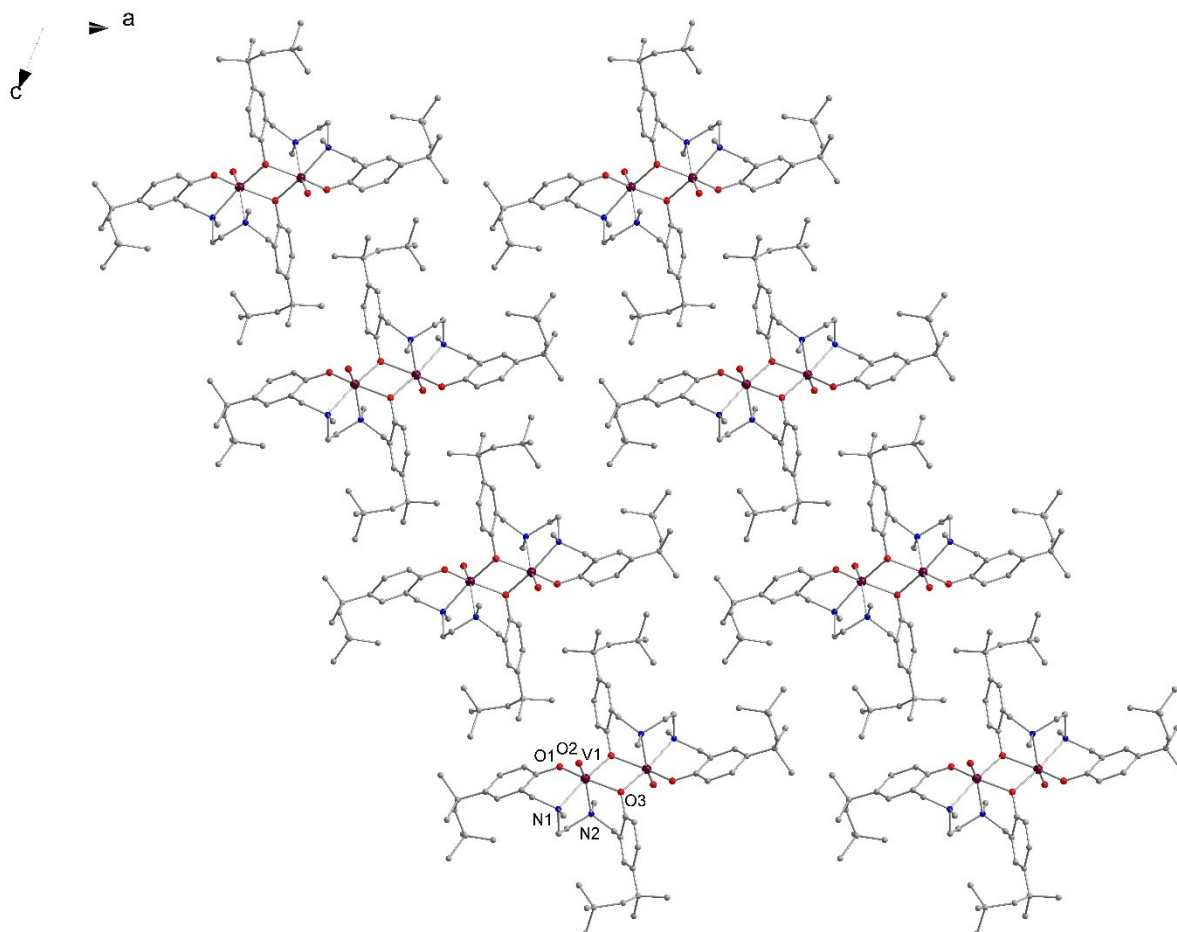


Figure S5. Arrangement of molecules **3** viewed down [010] direction. Only the higher occupation component of the disordered part was depicted. H atoms have been omitted for clarity.

Table S8. Geometry of C–H \cdots π interactions in **3**.

C–H \cdots π	H \cdots Cg (Å)	C \cdots Cg (Å)	\angle (C–H \cdots Cg) (°)
C8–H8C \cdots Cg4	2.83	3.75	158
C11–H11B \cdots Cg1	2.98	3.33	102
C11 ⁱ –H11B \cdots Cg1	2.98	3.33	102

Symmetry codes: [i] 1-x, 1-y, 1-z
 Cg1 [V1/O3/V1ⁱ/O3ⁱ]; Cg4 [C13/C14/C15/C16/C17/C18]

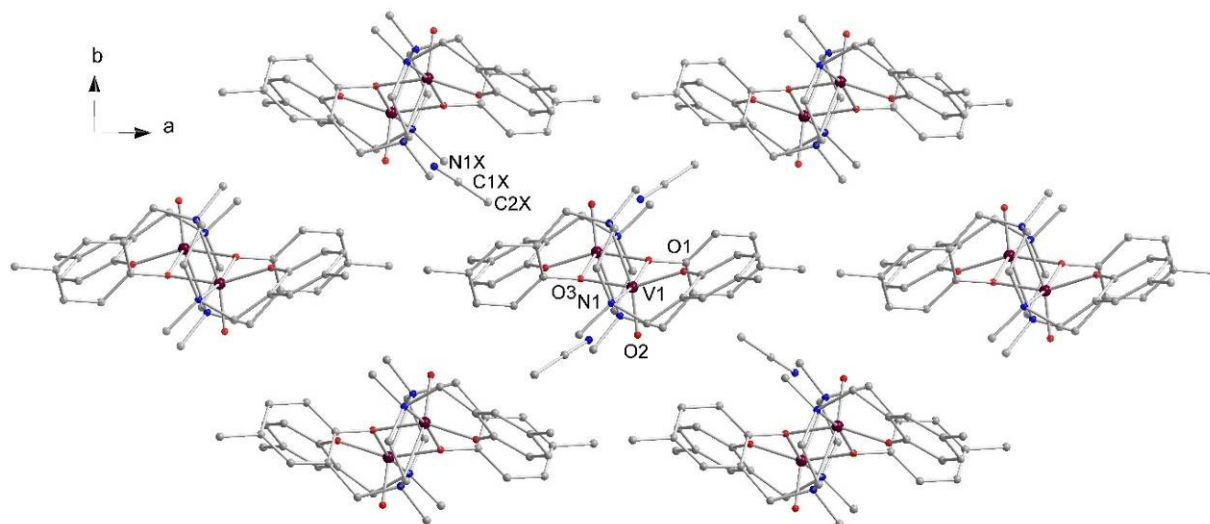


Figure S6. Packing diagram presenting selected molecules of $4 \cdot 2\text{CH}_3\text{CN}$ arranged in layers parallel to the (010) plane. Molecules of CH_3CN are located between layers. H atoms have been omitted for clarity.

Table S9. Geometry of C–H \cdots π interactions in **4**.

C–H \cdots π	H \cdots Cg (Å)	C \cdots Cg (Å)	\angle (C–H \cdots Cg) (°)
C8–H8C \cdots Cg4	2.66	3.61	162
C11–H11B \cdots Cg1	2.97	3.31	102
C11–H11B \cdots Cg1 ⁱ	2.97	3.31	102
C2X–H22A \cdots Cg4	2.73	3.51	137

Symmetry codes: [i] 1-x, 1-y, 1-z

Cg1 [V1/O3/V1ⁱ/O3ⁱ]; Cg4 [C13/C14/C15/C16/C17/C18]

Table S10. Geometry of intermolecular hydrogen bonds in **4**.

	D–H (Å)	H \cdots A (Å)	D \cdots A (Å)	\angle (D–H \cdots A) (°)
C7–H7A \cdots N1X	0.99	2.60	3.519(3)	155

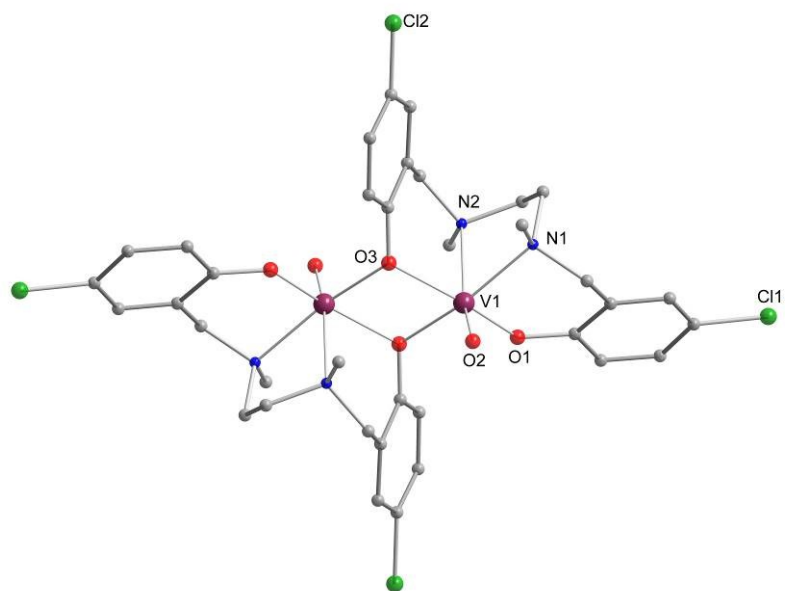


Figure S7. The molecular structure of $5 \cdot 2\text{CH}_3\text{CN}$ with crystallographic numbering of the donor atoms. Hydrogen atoms and CH_3CN molecules are omitted for clarity.

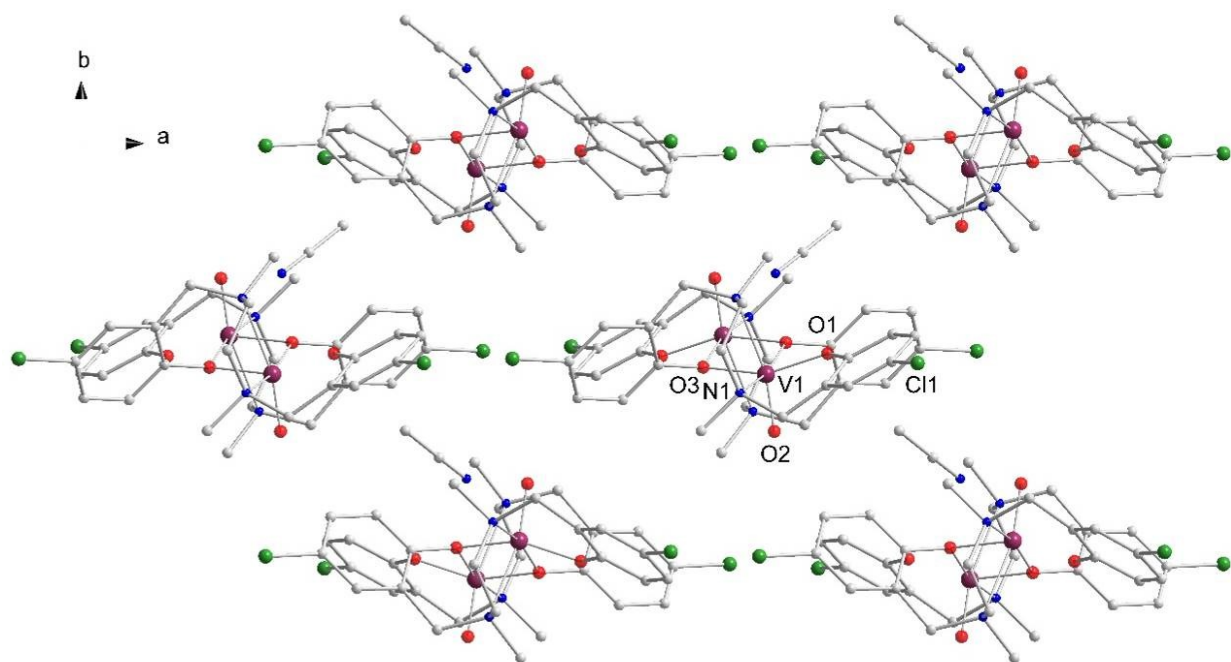


Figure S8. Arrangement of molecules $5 \cdot 2\text{CH}_3\text{CN}$ viewed down $[001]$ direction. H atoms have been omitted for clarity.

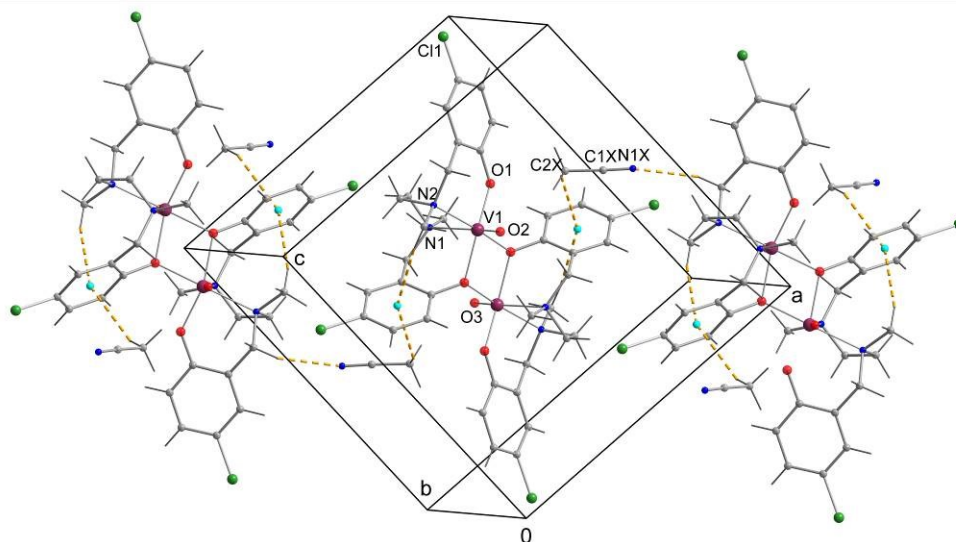


Figure S9. A chain of molecules in **5** held together by C–H \cdots π interactions (C2 $_x$ –H2B \cdots Cg6 i and C8–H8C \cdots Cg6, $i = 1-x, 1-y, 1-z$ and hydrogen bond (C7–H7A \cdots N1X ii , $ii = -1/2+x, 1/2-y, 1/2+z$) (marked by yellow dashed line). The centroids are shown as blue balls.

Table S11. Geometry of C–H \cdots π interactions in **5**.

C–H \cdots π	H \cdots Cg (Å)	C \cdots Cg (Å)	\angle (C–H \cdots Cg) (°)
C2X–H2B \cdots Cg6 i	2.68	3.47	138
C8–H8C \cdots Cg6	2.63	3.57	162
C11–H11B \cdots Cg1	2.97	3.31	101
C11–H11B \cdots Cg1 i	2.97	3.51	101

Symmetry codes: [i] 1-x, 1-y, 1-z
 Cg1 [V1/O3/V1 i /O3 i]; Cg6 [C13/C14/C15/C16/C17/C18]

Table S12. Geometry of intermolecular hydrogen bonds in **5**.

	D–H (Å)	H \cdots A (Å)	D \cdots A (Å)	\angle (D–H \cdots A) (°)
C7–H7A \cdots N1X ii	0.99	2.53	3.456(3)	155

Symmetry codes: [ii] -1/2+x, 1/2-y, 1/2+z

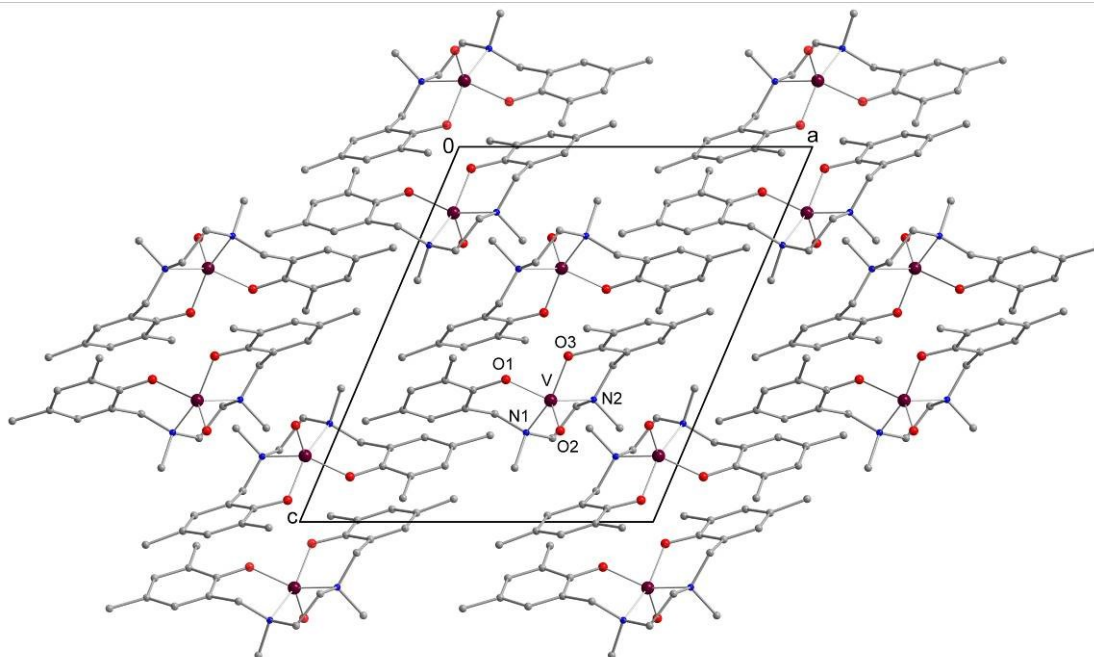


Figure S10. Packing diagram in **6** viewed down the [010] direction. H atoms have been omitted for clarity.

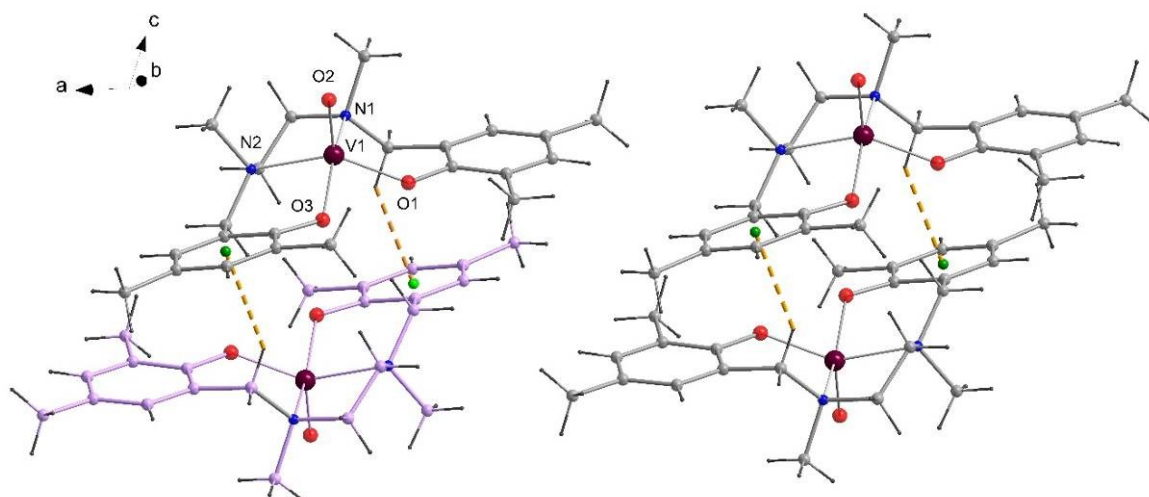


Figure S11. C–H \cdots π interactions in **6** (marked by yellow dashed line). Centroids are shown as green balls.

Table S13. Geometry of C–H \cdots π interactions in **6**.

C–H \cdots π	H \cdots Cg (Å)	C \cdots Cg (Å)	\angle (C–H \cdots Cg) (°)
C7–H7B \cdots Cg5 ⁱ	2.63	3.44	139
Symmetry codes: [i] 1-x, 1-y, 1-z			
Cg5 [C13/C14/C15/C16/C17/C18]			

Table S14. Geometry of $\pi\cdots\pi$ interactions in **6**.

C-H $\cdots\pi$	Cg \cdots Cg (\AA)	$\angle(\text{Gamma})$ ($^\circ$)
Cg4 \cdots Cg5 ⁱ	4.28	44
Cg5 \cdots Cg4 ⁱ	4.28	33

Symmetry code: [i] 1-x, 1-y, 1-z

Cg4 [C1/C2/C3/C4/C5/C6]; Cg5 [C13/C14/C15/C16/C17/C18];

$\angle(\text{Gamma}) = 44^\circ$ is the angle formed between the vector connecting centers of the rings Cg(4) \cdots Cg(5)ⁱ and normal to the plane of Cg5

$\angle(\text{Gamma}) = 33^\circ$ is the angle formed between the vector connecting centers of the rings Cg(5) \cdots Cg(4)ⁱ and normal to the plane of Cg4

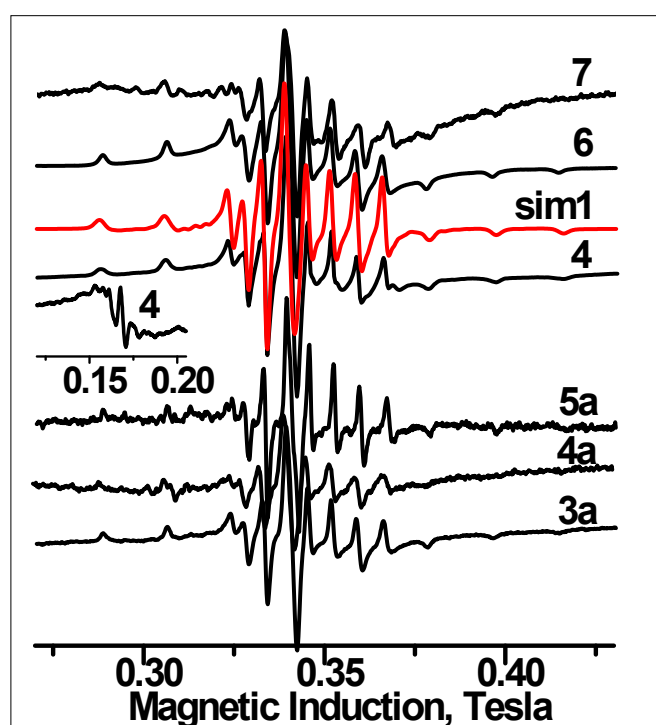


Figure S12. Frozen solution EPR spectra (at 77 K) of compounds 3–7 (4 in CH_2Cl_2 , 3a- 5a correspond to 3-5 in CH_3CN ; 6 and 7 in CH_2Cl_2) together with the theoretical spectrum sim1, calculated by using the parameters given in the text.

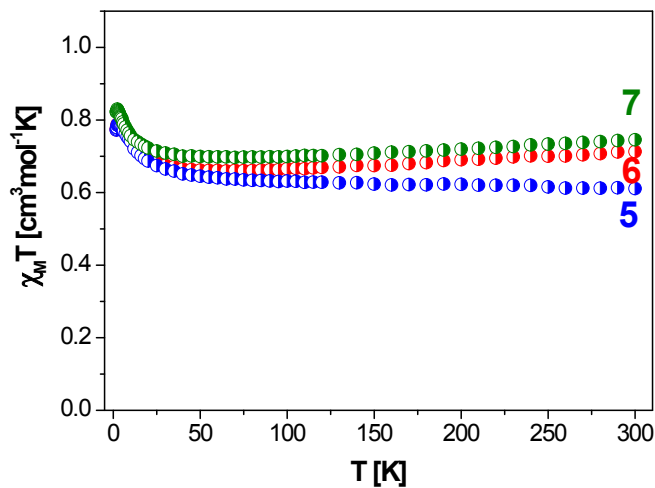


Figure S13. The $\chi_M T$ vs T product after subtracting TIP from the experimental data for **3–5**.

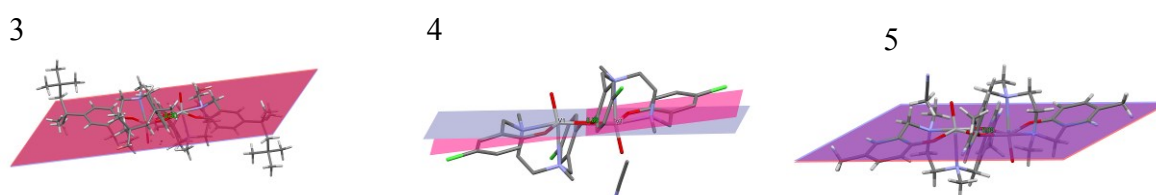


Figure S14. Dihedral angle between the two V_2O_2 planes for **3–5**.

Table S15. Magnetic and structural parameters for binuclear octahedral oxidovanadium(IV) compounds.

Compound	J/cm^{-1} (T/K)	$V \cdots V$ /Å	$V-O-V/^\circ$	$\tau/^\circ$	Ref.
$[\text{Et}_3\text{NH}]_2[(\text{VO})_2\text{L}] \cdot 4\text{CH}_2\text{Cl}_2^a$	-167.9	3.125	98.6	180^b	24a
$[(\text{VO})_2(\text{L}^2)(\text{OCH}_3)(\text{DMSO})]^c$	-244 ^d	3.026	94.3, 101.8	131.1^b	24b
$[(\text{VO})_2(\text{L}^3)(\text{OH})_2]\text{I}_2 \cdot 4\text{H}_2\text{O}^e$	-300 ^d	2.965	98.1	175.7^b	24c
$[(\text{VO})_2(\text{L}^4)(\text{OH})_2]\text{Br}_2^f$	-354 ^d	3.033	101.2	180^b	24d
5	+0.40	3.243	106.9	180	This work
6	+5.34	3.249	106.5	174.1	This work
7	+3.22	3.254	106.1	180	This work
$[(\text{VO})_2(\text{HL}^5)_2]^g$	+3.1	—	107.0	0.0^b	2c

^aH₃L¹ = (*N,N*-bis(2-hydroxybenzyl)amino)acetic acid), ^bRef. 24a,

^cL² = 2,6-bis-(salicylideneaminomethyl)-4-methylphenol, ^d*J* converted to the convention $-JS_1S_2$ used in this paper.

^eL³ = *N,N,N,N*-tetrakis(2-pyridylmethyl)-ethylenediamine, ^fL⁴ = 1,4,7-triazacyclononane,

^gH₃L⁵ = *N*-salicylidene-2-[bis(2-hydroxyethyl)amino]ethylamine.

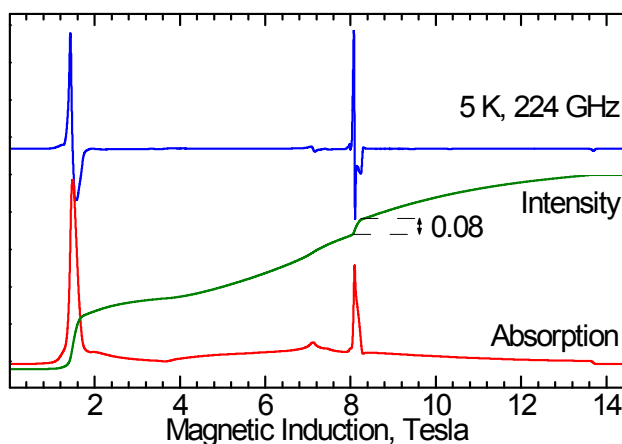


Figure S15. Blue: HFEPR spectrum of **1**. Red: integrated spectrum - absorption. Green: integrated absorption - intensity. The V(IV) contamination contributes 8% of the total EPR intensity (the vertical range of the intensity plot is 0 to 1).

Monomeric V(III) and V(IV) Compounds.

Magnetic properties for polycrystalline samples of monomeric non-oxidovanadium(III) **1**, **2** and oxidovanadium(IV) **6**, **7** are presented in Figure S16 –S18.

Compounds **1** and **2** exhibit large zero-field splitting. To take this into account, the magnetic susceptibility may be calculated from the fundamental formula

$$\chi_{V(III)} = -\frac{N \sum_i \frac{\partial E_i}{\partial B} e^{-\frac{E_i}{kT}}}{B \sum_i e^{-\frac{E_i}{kT}}} + TIP \quad (S1)$$

The three energies E_i of the triplet state were determined by diagonalizing the matrix of the spin-Hamiltonian. The $\frac{\partial E_i}{\partial B}$ derivatives were calculated numerically, by evaluating energies E_i 5 Gauss below and 5 Gauss above the magnetic field of the the SQUID instrument (5000 G). Formula (S1) gives the magnetic susceptibility χ at an orientation (Θ , Φ) of a molecule versus the magnetic field and needs still to be averaged over all orientations, which is accomplished by numerical integration of $\chi(\Theta, \Phi) \sin \Theta d\Theta d\Phi$, in similar way as powder EPR spectra are calculated. Both V(III) complexes contain substantial V(IV) contamination seen in EPR (Figure S15) whose magnetic susceptibility was expressed as

$$\chi_{V(IV)} = \frac{N\mu_B^2 g^2}{3kT} \frac{3}{4} \quad (S2)$$

The equation for total susceptibility was

$$\chi = (1 - x)\chi_{V(III)} + x\chi_{V(IV)} \quad (S3)$$

where x is the fraction of the V(IV) contamination.

Finally, the effect of the intermolecular interactions was taken into account by converting the susceptibility above to

$$\chi' = \frac{\chi}{1 - \frac{2zJ\chi}{N\mu_B^2 g^2}} \quad (S4)$$

The g , D and E parameters were not fitted, they were fixed at values found from EPR. Only the fraction of the V(IV) impurities, zJ and TIP were allowed to vary. The results are presented in Figures S16 and S17.

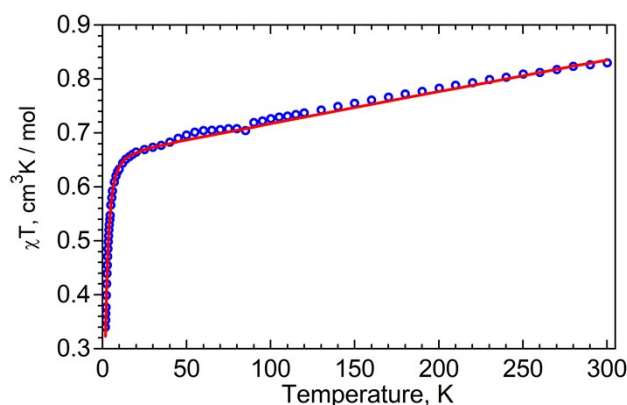


Figure S16. Magnetic data for **1**. Blue:experimental points. Red: calculated using $g_{\text{ave}}=1.94$, $D=5.29 \text{ cm}^{-1}$, $E=1.68 \text{ cm}^{-1}$, 30% of the V(IV) impurity, $zJ=0.0085 \text{ cm}^{-1}$, $TIP=588 \cdot 10^{-6} \text{ cm}^3\text{mol}^{-1}$. D and E are the EPR values (see Figure 7, main text).

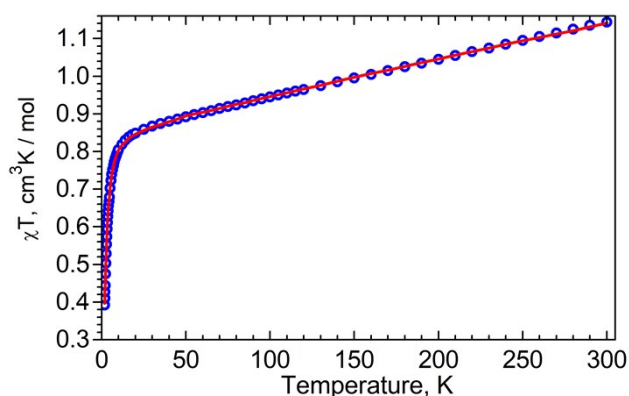


Figure S17. Magnetic data for **2**. Blue:experimental points. Red: calculated using $g_{\text{ave}} = 1.93$, $D = 5.26 \text{ cm}^{-1}$, $E = 1.67 \text{ cm}^{-1}$, 8.9 % of the V(IV) impurity, $zJ' = -0.14 \text{ cm}^{-1}$, $TIP=990 \cdot 10^{-6} \text{ cm}^3\text{mol}^{-1}$. D and E are the EPR values averaged for two species (see Figure 8, main text).

The simulation of magnetic data of **6** and **7**, shown in Figure S18, was carried out using the PHI program, taking into account the exchange zJ' and the TIP parameter. The fitting leads to the following results: $g = 1.94$ and $zJ' = -0.01 \text{ cm}^{-1}$, $TIP = 598 \cdot 10^{-6}$ for **6** and $g = 1.97$ and $zJ' = -0.08 \text{ cm}^{-1}$, $TIP = 441 \cdot 10^{-6}$ for **7**. Also as in case of **6** and **7**, very weak antiferromagnetic interaction in

the crystal lattice exist, in agreement with the X-ray studies (Figure S10 and S11; Table S13 and S14.)

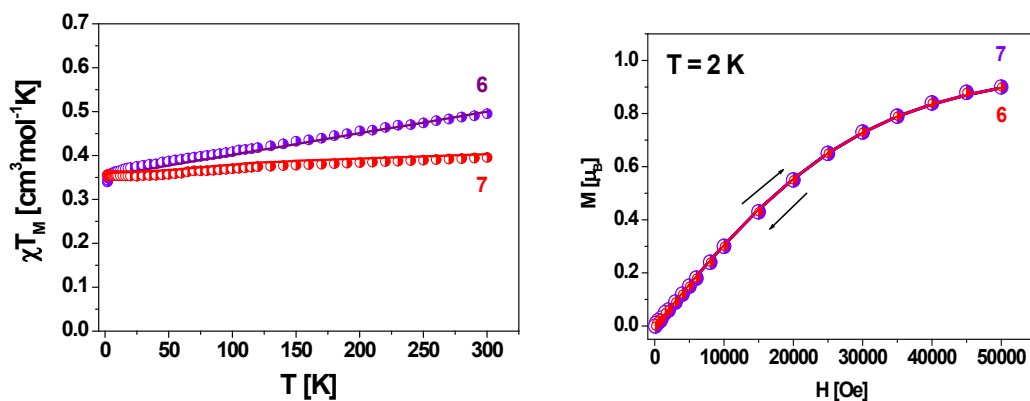


Figure S18. DC magnetic data for **6**, **7**. Left – (●) $\chi_M T$ and (○) χ_M . Right – field dependence of the magnetization per formula unit. The solid lines are calculated using the PHI program.